Large Contribution of Coarse Mode to Aerosol Microphysical and Optical Properties: Evidence from Ground-Based Observations of a Transpacific Dust Outbreak at a High-Elevation North American Site

E. KASSIANOV,[a] M. PEKOUR,[a] C. FLYNN,[a] L. K. BERG,[a] J. BERANEK,[a] A. ZELENYUK,[a] C. ZHAO,[a] L. R. LEUNG,[a] P. L. MA,[a] L. RIIHIMAKI,[a] J. D. FAST,[a] J. BARNARD,[b] A. G. HALLAR,[c,f] I. B. MCCUBBIN,[c] E. W. ELORANTA,[d] A. MCCOMISKEY,[e] AND P. J. RASCH[a]

[a] *Pacific Northwest National Laboratory, Richland, Washington*
[b] *University of Nevada, Reno, Nevada*
[c] *Storm Peak Laboratory, Desert Research Institute, Steamboat Springs, Colorado*
[d] *University of Wisconsin–Madison, Madison, Wisconsin*
[e] *National Oceanic and Atmospheric Administration, Boulder, Colorado*

(Manuscript received 1 September 2016, in final form 29 January 2017)

ABSTRACT

This work is motivated by previous studies of transatlantic transport of Saharan dust and the observed quasi-static nature of coarse mode aerosol with a volume median diameter (VMD) of approximately 3.5 μm. The authors examine coarse mode contributions from transpacific transport of dust to North American aerosol properties using a dataset collected at the high-elevation Storm Peak Laboratory (SPL) and the nearby Atmospheric Radiation Measurement (ARM) Mobile Facility. Collected ground-based data are complemented by quasi-global model simulations and satellite and ground-based observations. The authors identify a major dust event associated mostly with a transpacific plume (about 65% of near-surface aerosol mass) in which the coarse mode with moderate ($\sim$3 μm) VMD is distinct and contributes substantially to total aerosol volume (up to 70%) and scattering (up to 40%). The results demonstrate that the identified plume at the SPL site has a considerable fraction of supermicron particles (VMD $\sim$3 μm) and, thus, suggest that these particles have a fairly invariant behavior despite transpacific transport. If confirmed in additional studies, this invariant behavior may simplify considerably parameterizations for size-dependent processes associated with dust transport and removal.

1. Introduction

African and Asian deserts are major sources of dust particles lofted into the atmosphere. These particles, with an atmospheric lifetime ranging from several hours to several weeks, can be transported long distances from their source regions to areas located hundreds or even thousands kilometers away (Clarke et al. 2001; Obrist et al. 2008; Mahowald et al. 2014). Examples of such long-range transport include the summertime transatlantic transport of Saharan dust (Prenni et al. 2009; Nowottnick et al. 2011) and springtime transpacific transport of Asian dust (Wells et al. 2007; Cottle et al. 2013). These examples clearly demonstrate that dust emission, transport, and removal are not restricted to a given geographical region or period but are, rather, global phenomena.

Perhaps the greatest challenge to studying the evolution of dust properties during long-range transport is a lack of observations, particularly integrated datasets that permit assessment of the complex and size-dependent processes associated with dust emission, transport, and removal. Maring et al. (2003) analyzed the Saharan dust size distributions along a transatlantic transport pathway and provided some of the earliest observational evidence that the lifetime of supermicron particles is longer than expected from conventional deposition schemes. Over the subsequent decade, several studies (Reid et al. 2008; Ryder

[f] Additional affiliation: University of Utah, Salt Lake City, Utah.

Corresponding author e-mail: Evgueni Kassianov, evgueni.kassianov@pnnl.gov

DOI: 10.1175/JAS-D-16-0256.1

© 2017 American Meteorological Society. For information regarding reuse of this content and general copyright information, consult the AMS Copyright Policy (www.ametsoc.org/PUBSReuseLicenses).

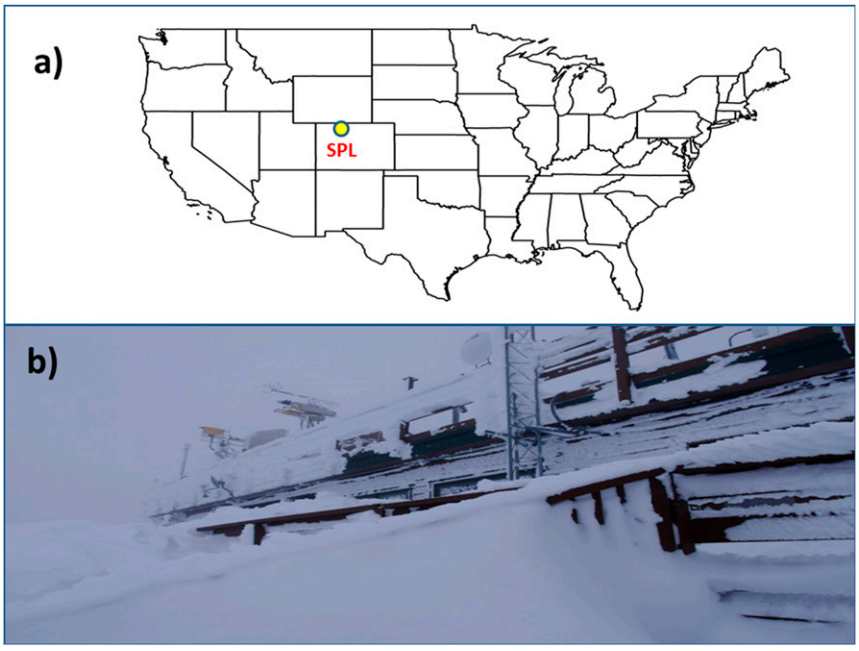

FIG. 1. (a) Map of North America with location of the SPL site (3.22 km MSL; 40.455°N, 106.745°W) and (b) typical image of the SPL site for a "cloudy" day in March 2011.

et al. 2013) confirmed and extended this finding. In particular, size distributions were sampled over different climate-important regions, such as the Arabian Gulf (Reid et al. 2008), Mauritania, and Mali (Ryder et al. 2013), influenced by dust transported from North Africa and the Middle East. Moreover, Ryder et al. (2013) assembled measured particle size distributions from five major aircraft campaigns and demonstrated that there is a good overlap between these distributions at sizes smaller than 3 μm despite different source regions and travel times. Among other interesting results, Reid et al. (2008) indicated that the dust coarse mode, with a volume median diameter (VMD) of approximately 3.5 μm and a standard deviation of 30%, appears fairly invariant over the processing time from different sources for the short-to-moderate travel period.

However, these findings on the striking quasi-static behavior of the dust coarse mode over the transport processing time remain inconclusive, because the previous studies did not focus on the western United States with frequent orographic precipitation. Wet deposition includes in-cloud and below-cloud scavenging and is strongly dependent on particle size (Rasch et al. 2000). Using below-cloud scavenging by rain and snow as an example, it has been shown that values of the scavenging coefficient for large particles ($PM_{2.5–10}$) are about two orders of magnitude larger than those for smaller particles ($PM_{2.5}$) (Wang et al. 2014). Since African and Asian dust associated with transpacific transport appears to be an important factor in the orographic precipitation processes over mountainous western United States (Creamean et al. 2013; Fan et al. 2014), wet deposition likely modifies the particle size distribution inside dust-rich layers that traversed these areas. Thus, it is unclear whether or not the coarse mode aerosol is an important contributor to the overall aerosol properties of these elevated layers.

The purpose of this paper is twofold. First, we identify a significant event with transpacific dust at a remote high-elevation site using an integrated dataset of aerosol properties and output from a chemical transport model. Second, we demonstrate that the coarse mode (VMD $\sim$ 3 μm) is indeed well defined and contributes strongly to aerosol microphysical and optical properties. We also discuss similar behavior of the coarse mode during transpacific and transatlantic transport of dust.

2. Data and model

We use datasets collected from surface-based observations during the Storm Peak Laboratory (SPL) Cloud Property Validation Experiment (STORMVEX; Marchand et al. 2013) at high-elevation, mountain-top atmospheric research facilities in Colorado (Fig. 1). During STORMVEX, the Atmospheric Radiation Measurement (ARM) Climate Research Facility Mobile Facility (AMF; https://www.arm.gov/sites/amf) was deployed at the Thunderhead Lodge site [S1; 2.76 km

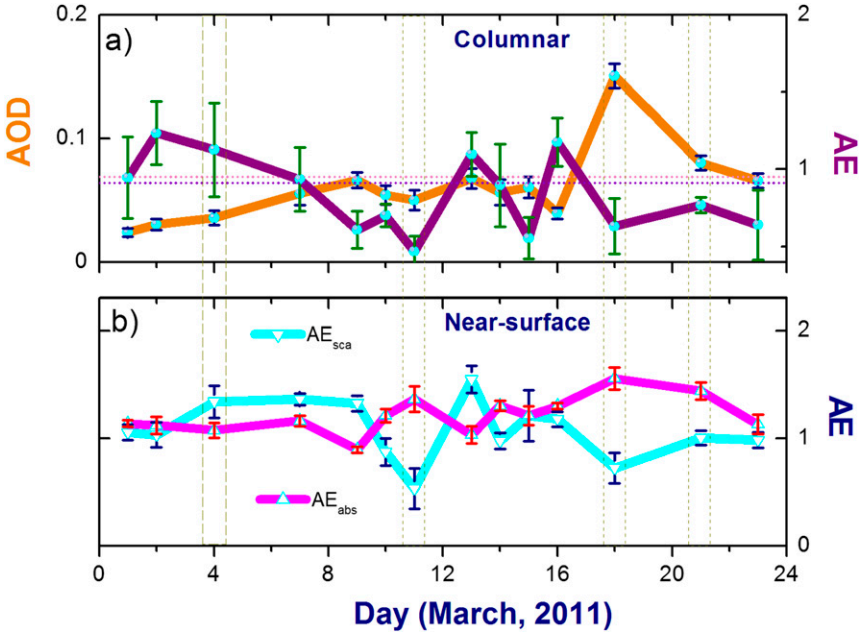

FIG. 2. (a) Column aerosol properties derived from MFRSR data: Time series of daily averaged AOD at 0.5-μm wavelength (orange solid line) and AE (0.50/0.87 μm) (purple solid line). The corresponding multiyear spring-averaged values (Hallar et al. 2015) are included as well (horizontal dotted lines). (b) In situ near-surface aerosol properties (nephelometer and PSAP data): Time series of daily averaged AE (0.45/0.7 μm) for total scattering (cyan line) and absorption (magenta line). Error bars represent variability of the optical properties. Four days of interest (4, 11, 18, and 23 Mar) are identified by vertical dashed lines.

above mean sea level (MSL)] located approximately 2.4 km west of the mountain-top SPL (3.22 km MSL; http://stormpeak.dri.edu/). Although the overall time period of the STORMVEX is about 5 months (from 1 November 2010 to early April 2011), only data from March 2011 are discussed here. Availability of clear-sky aerosol retrievals and high-quality in situ aerosol measurements are the main criteria for selection of the period of interest.

The AMF site was equipped with a suite of instruments for measuring cloud and aerosol radiative properties, including a Multifilter Rotating Shadowband Radiometer (MFRSR) and the University of Wisconsin (UW) High Spectral Resolution Lidar (HSRL). The MFRSR measures the total all-sky surface downwelling irradiance and its diffuse and direct components at six wavelengths (0.415, 0.5, 0.615, 0.673, 0.87, and 0.94 μm). The aerosol optical depth (AOD) is derived from the spectrally resolved measurements of direct irradiance (Harrison et al. 1994) at the first five of these wavelengths. Similar to Michalsky et al. (2010), cloud screening is applied to remove cloud-contaminated AODs. The UW HSRL provides vertical profiles of aerosol backscatter cross section and particulate linear depolarization ratio (Eloranta 2005). Since the depolarization ratio is a good discriminator for nonspherical particles and large dust particles typically have nonspherical geometry (Pan et al. 2015), we use the HSRL depolarization ratio for identification of possible dust events.

The SPL site was equipped with a suite of instruments for sampling near-surface aerosol microphysical, chemical, and optical properties. The suite includes a scanning mobility particle sizer (SMPS; mobility size range: 0.012–0.4 μm), an aerodynamic particle sizer (APS; aerodynamic size range: 0.5–20 μm), particle soot/absorption photometer (PSAP), a TSI integrating nephelometer, and a single-particle mass spectrometer (SPLAT II). We calculate the contribution of the supermicron particles (aerodynamic diameter >1 μm) to total volume using the SMPS and APS size distributions. The TSI integrating nephelometer measures the total scattering coefficient at three wavelengths (0.45, 0.55, and 0.7 μm), while the PSAP measures light absorption coefficient at three wavelengths (0.467, 0.53, and 0.66 μm). We adjust the nephelometer data using the measured Angstrom exponent (AE) for light scattering to match the PSAP wavelengths. Both the nephelometer and PSAP include 1- and 10-μm impactors. We calculate the contribution of supermicron particles to the light

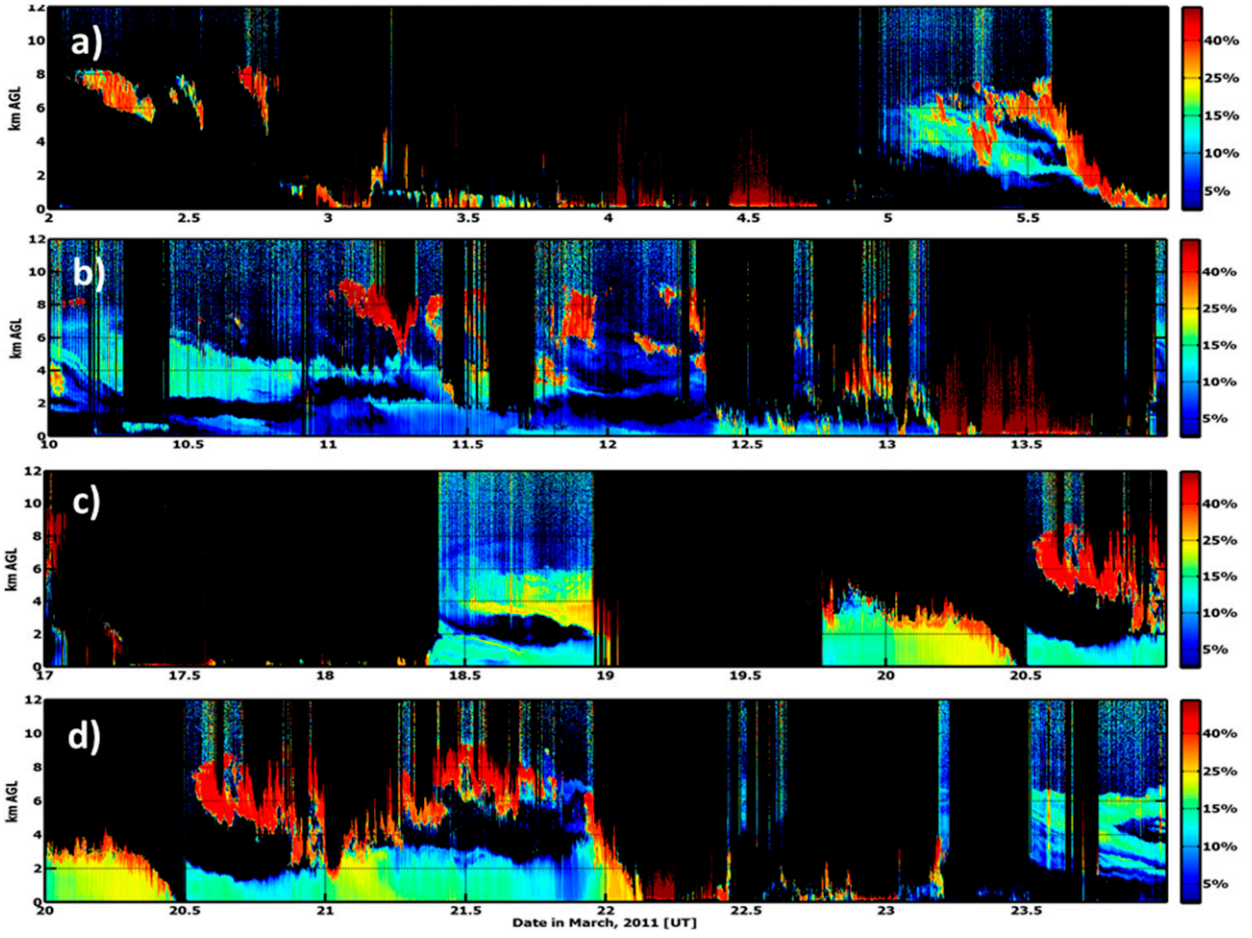

FIG. 3. Time–height images of particulate linear depolarization ratio derived from the HSRL for 4-day periods in March 2011 around 4 days: (a) 4, (b) 11, (c) 18, and (d) 21 Mar; horizontal axis is time (calendar date in March 2011, UTC) and vertical axis is altitude (km). Increasing color wavelength (blue to yellow to red) represents increasing particulate depolarization ratio, which in turn indicates departure from sphericity (from minute spherical particles to irregularly shaped aerosol particles and ice crystals). Black color includes three main categories: 1) small near-spherical particles or clear air having depolarization ratio below 5% (e.g., the end of 4 Mar), 2) low signal to noise of clear air or by signal attenuation caused by a dense lower layer (e.g., black features above a layer with red; the end of 5 Mar), and 3) instrument malfunction (seed laser wavelength lock failure) that makes it impossible to report confident calibrated quantities (e.g., midday 19 Mar). Occasionally (e.g., midday 13 Mar) depolarization ratios greater than 60% extending from the ground level to several kilometers appear when the beam is completely extinguished at near-ground level. These features (dark red) are artificial and should be disregarded.

scattering and absorption using the nephelometer and PSAP measurements with 1- and 10-μm cutoffs, respectively. SPLAT II provides the size and internal composition of individual particles in the 0.05–3-μm size range, with a 50% cutoff point at about 0.085 μm (Zelenyuk et al. 2015). We use this chemical characterization to augment the HSRL and help in the identification of possible dust events.

Two models are used to examine dust transport to an area (about 1° × 1°) surrounding the SPL site for the period of interest (March 2011): the Weather Research and Forecasting (WRF) Model, coupled with chemistry (WRF-Chem), and the Community Atmosphere Model, version 5 (CAM5). In particular, we use a subset of the quasi-global (67.5°S–77.5°N, 180°W–180°E) 5-yr (2010–14) WRF-Chem simulations (Hu et al. 2016) nudged with National Centers for Environmental Prediction Final Analysis (NCEP FNL). We also explore the dust transport using a 1° × 1° CAM5 simulation nudged with the Modern Era Reanalysis for Research and Applications (MERRA) following Ma et al. (2015). A detailed evaluation of aerosol properties simulated by WRF-Chem is provided in Hu et al. (2016), with a focus on the transpacific transport that utilized extensively integrated satellite and ground-based observations. The latter included data from the Aerosol Robotic Network

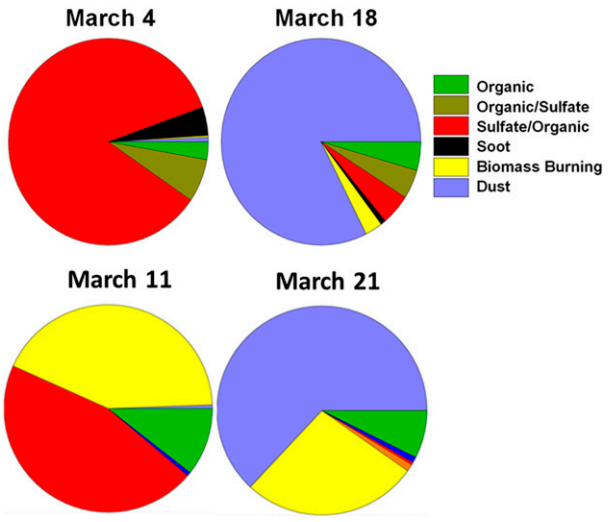

FIG. 4. Relative fractions of individual particles with different chemical composition characterized with SPLAT II for 4 days in March 2011: (top left) 4, (bottom left) 11, (top right) 18, and (bottom right) 21 Mar. In comparison with 18 Mar (top right), 11 Mar (bottom left) is characterized by an increased amount of biomass-burning particles: about 40% (11 Mar) vs about 5% (18 Mar).

(AERONET; http://aeronet.gsfc.nasa.gov; Holben et al. 1998) and the Interagency Monitoring of Protected Visual Environments (IMPROVE; http://vista.cira.colostate.edu/Improve/; Malm et al. 1994) networks, while the combined satellite observations featured AOD from the Moderate Resolution Imaging Spectroradiometer (MODIS) aboard the NASA's *Terra* satellite (Levy et al. 2013) and aerosol extinction profiles from the Cloud–Aerosol Lidar with Orthogonal Polarization (CALIOP) lidar on board the *Cloud–Aerosol Lidar and Infrared Pathfinder Satellite Observations* (*CALIPSO*) (Winker et al. 2009). The WRF-Chem simulations (Hu et al. 2016) generally reproduce both spatial and seasonal variations of aerosol properties, such as AOD and the vertical distribution of aerosol extinction. For example, the simulated AODs are mostly (~90%) within a factor of 2 of the AERONET AODs, while the simulated variations of aerosol extinction are in good agreement (correlation coefficient ~0.95–0.97) with the *CALIPSO* data. Recent evaluation of the aerosol properties simulated by the CAM5 model (Liu et al. 2012) is also encouraging because of the reasonable agreement (the normalized mean bias is −0.29) between the simulated and AERONET monthly AODs in North America and because of the similar global pattern of the simulated and satellite AODs (Kinne et al. 2006). Since the WRF-Chem and CAM5 simulations have demonstrated reasonable skill in simulating aerosol properties against observations, we use the model outputs to estimate the relative contribution of the transpacific transport of Asian and African dust to the major dust event identified by the ground-based observations at the SPL site.

3. Results and discussion

We start with identification of the major dust event (Figs. 2–4), continue with dust source characterization (Fig. 5), and then discuss the contribution of the supermicron particles to aerosol microphysical and optical properties (Fig. 6). We identify these contributions as coarse mode fractions (CMFs) of aerosol properties. Appendix A provides spatial distribution of AOD and precipitation simulated by WRF-Chem and CAM5 for the selected dust episode, while appendix B offers an observational support of the WRF-Chem simulations using both MODIS and *CALIPSO* data.

There are four conventional approaches for identifying dust events. The first approach utilizes two parameters (AOD and AE) that describe aerosol loading and particle size. While large (>0.5) AODs at 0.5-μm wavelength and small (<0.5) AEs (computed between 0.5 and 0.87 μm) are associated with dust episodes near sources (e.g., Slingo et al. 2006), small-to-moderate AODs (<0.15) and small-to-moderate AEs (<1) can also be associated with regional and transcontinental dust events at the remote high-altitude SPL site (Hallar et al. 2015). The second approach utilizes AEs defined for light scattering and absorption at 0.44- and 0.675-μm wavelengths; small-to-moderate scattering AEs (<1) and moderate-to-large absorption AEs (>1.5) indicate predominance of dust (Cazorla et al. 2013). The other two approaches utilize the depolarization ratio and chemical composition from the HSRL and SPLAT II data, respectively.

Similar to Hallar et al. (2015), we use the first two approaches to identify 18 March as a representative "dusty" day (Fig. 2). In particular, the corresponding values of the near-surface scattering AE and absorption AE (Fig. 2b) are distinctive fingerprints of dust on 18 March. Additional evidence of dust aerosol on 18 March is provided by 1) quite large values (up to 0.3) of HSRL-measured particulate linear depolarization ratio (Fig. 3c) and 2) chemical composition of individual aerosol particles obtained from SPLAT II (Fig. 4). About 82% of the particles characterized with SPLAT II are identified as dust for the dusty day (Fig. 4). The pie charts shown in Fig. 4 are based on a statistically robust sample that consist of ~175 000 single-particle mass spectra, which in turn are classified into different aerosol classes. Note that these pie charts present relative number fractions of particles with different compositions and, therefore, predominantly

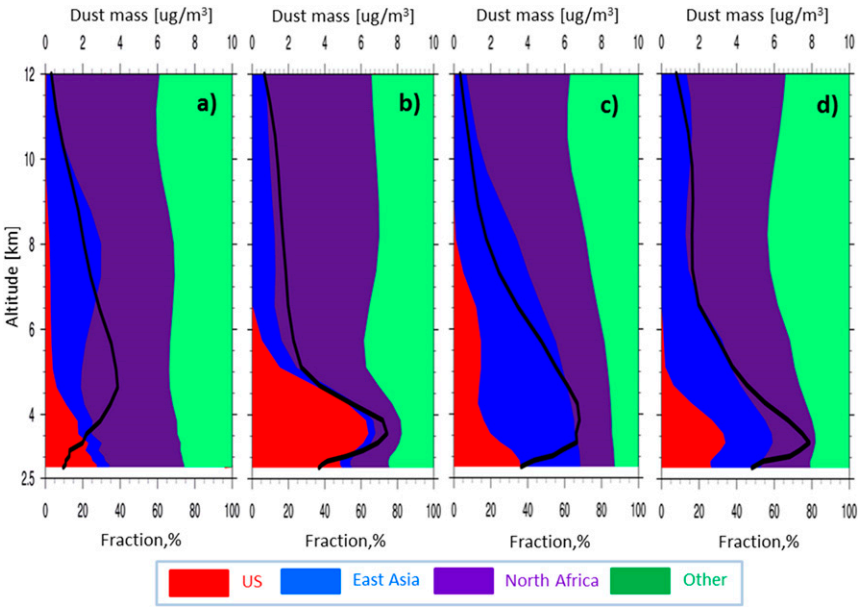

FIG. 5. WRF-Chem-simulated fraction of dust mass as a function of source and altitude (colors) and total mass (solid line) for 4 days in March 2011: (a) 4, (b) 11, (c) 18, and (d) 21 Mar. The label ''other'' defines other major Asian–Arabian sources of dust located between eastern Asia and North Africa. The WRF-simulated fraction of dust mass shows substantial day-to-day variability. In comparison with 18 Mar (c), 11 Mar (b) is characterized by larger contribution from local sources: about 50% (11 Mar) vs about 35% (18 Mar) near ground level. The opposite is true for 21 Mar (d): about 25% (21 Mar) vs about 35% (18 Mar).

reflect composition of submicron particles, which represent over 99% of particle number concentration. Nevertheless, the SPLAT II data clearly indicate that on 18 March the majority of aerosol particles were composed of dust. The WRF-Chem simulations (Fig. 5c) indicate that remote African and Asian areas are the major sources (~65% of simulated near-surface dust mass) of the dust observed at the SPL site. Supermicron particles contribute mostly to the volume for the dusty day (Fig. 6a), and the corresponding VMD is about 3 μm (Fig. 6c). The large fraction of these particles (Fig. 6a) is responsible for the noticeable difference between the measured aerosol optical properties with 1- and 10-μm cutoffs (Fig. 6b) and the corresponding moderate-to-large values of CMF (Fig. 6d). The latter are about 25%, 40%, and 70% for the total absorption, scattering, and volume, respectively.

A little more insight into the application of the second approach (Cazorla et al. 2013) can be gained if we consider two additional days of interest (11 and 21 March). According to this approach, large and absorbing particles, such as black carbon particles with a sulfate coating (e.g., Lack and Cappa 2010), seem to influence the observed aerosol properties on 11 March, while large and weakly absorbing particles, such as dust, appear to dominate on 21 March (Fig. 2b). The suggested classification of aerosol type (absorbing vs weakly absorbing particles) is consistent with the corresponding classification provided by the depolarization ratio (Fig. 3) and chemical composition (Fig. 4). For example, the near-surface values of the depolarization ratio are about 10% and 20% on 11 March (Fig. 3b) and 21 March (Fig. 3d), respectively. Since biomass-burning particles tend to have low values of the depolarization ratio (e.g., de Foy et al. 2011; Burton et al. 2015), the substantial amount of biomass-burning particles on 11 March (Fig. 4) contributed at least in part to the observed ratio reduction (11 vs 21 March). Note that the typical value of the depolarization ratio at 0.532-μm wavelength is about 0.09 for smoke sampled within an area surrounding the SPL site (near Denver) and about 0.3 for the Saharan dust transported to the Midwest United States (Burton et al. 2015). It is quite interesting that a peak of the depolarization ratio (~0.3) occurred within an elevated layer (~4 km) on 18 March (Fig. 3c), which is likely characterized by a large contribution (~85% of simulated dust mass from about 4 to 6 km) of dust transported from remote African and Asian areas (Fig. 5c). It should also be emphasized that the second approach (Cazorla et al. 2013) is based on near-surface

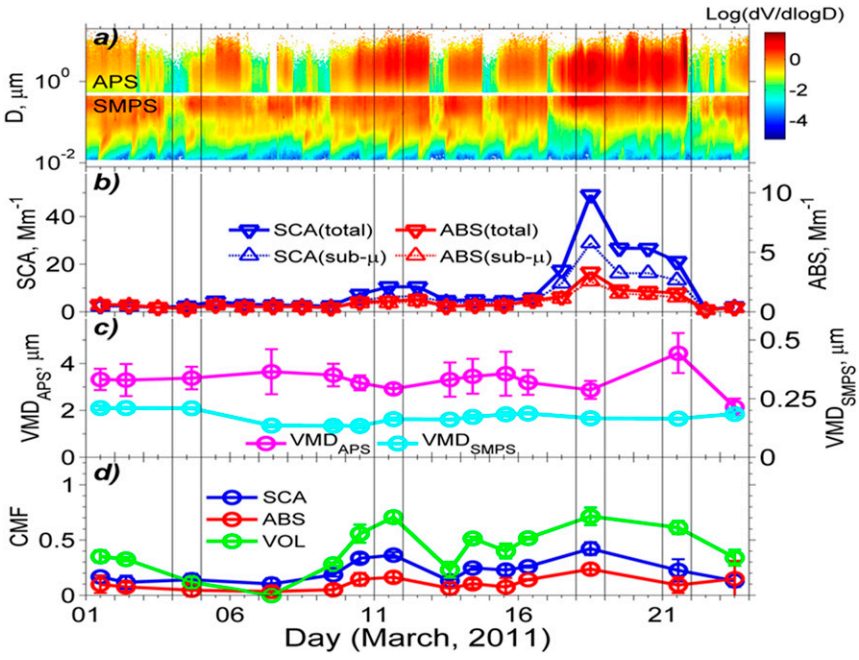

FIG. 6. Time series of (a) combined APS and SMPS volume size distributions, the daily averaged values of (b) total scattering (SCA) and absorption (ABS) coefficients measured with 1- (thin dotted lines) and 10-μm (thick solid lines) cutoffs at 0.55- and 0.53-μm wavelengths by TSI integrating nephelometer and PSAP, respectively, (c) VMD estimated from the SMPS (cyan) and APS (magenta) data, and (d) CMF for total volume (VOL) and total scattering and absorption at 0.55- and 0.53-μm wavelengths, respectively. Note that the daily averaged values of VMD in (c) and CMF in (d) are calculated for the same periods as those for AOD and AE (Fig. 2).

data, while the first approach (e.g., Hallar et al. 2015) incorporates columnar aerosol properties.

A distinct dust coarse mode (with VMD on the order of ~6 μm) is common at the Semi-Arid Climate Observatory and Laboratory (SACOL, located in China at 35.57°N, 104.08°E; 1.97 km MSL) during the springtime when frequent Asian dust storms have strong influence on regional aerosol properties (Chen et al. 2014). The AERONET-retrieved VMD is about 5 μm at the SACOL site on 11 March 2011 (appendix C) and, thus, compares well with its climatological value (~6 μm). The remote North American mountain-top SPL site, located thousands kilometers away from major Asian sources, shows a well-defined dust coarse mode (Fig. 6a) with smaller VMD (~3 μm) (Fig. 6c) for the identified dusty day (18 March 2011). For this day, the AERONET-retrieved VMD is also about 3 μm at the Boulder site in the vicinity SPL site (appendix C) and thus matches the corresponding SPL VMD. This difference between the local and remote VMDs (~5 μm at the SACOL site vs ~3 μm at the SPL site) suggests that distribution of supermicron dust particles evolve to smaller diameters during the transpacific journey of dust. These results are in line with findings from previous studies (Maring et al. 2003; Reid et al. 2008; Ryder et al. 2013).

Since our results rely on 1 month of integrated observations at two nearby mountain-top sites, additional efforts that combine both observational and model components are required. However, if the projected robustness of the coarse mode during long-range transport is confirmed, it will become easier to address important issues associated with understanding the short- and long-term effects of dust on atmospheric chemistry, aerosols, and radiation. For example, a fairly invariant behavior of coarse mode dust aerosols could lead to the development of simplified parameterizations that represent complex and size-dependent processes associated with dust transport and removal. Improved understanding is needed to draw conclusions about the influence of dust on aerosol radiative forcing and dust-related impacts to climate change at both the regional and global scales (Prenni et al. 2009; Choobari et al. 2014).

4. Summary

Evidence from an integrated dataset collected during the Storm Peak Laboratory (SPL) Cloud Property

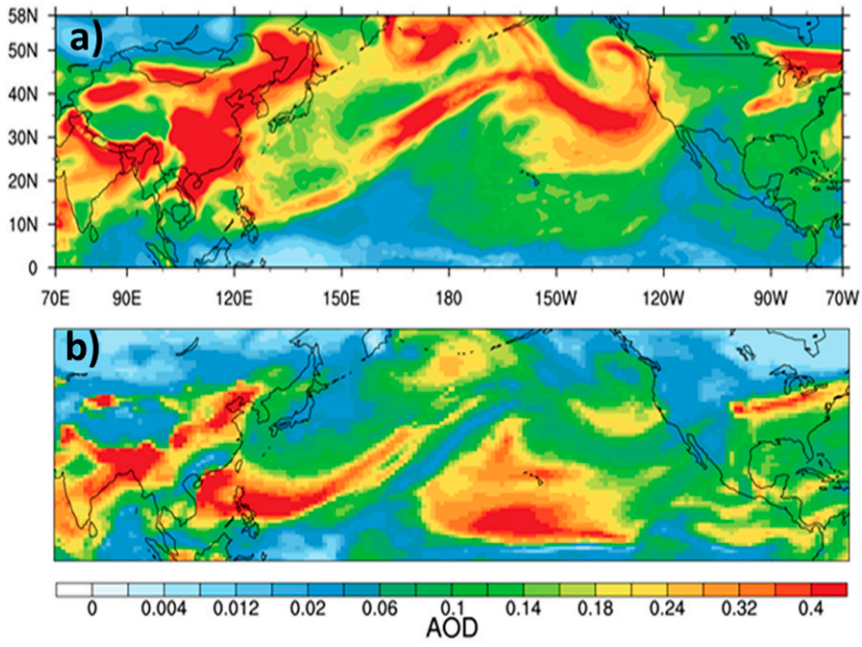

FIG. A1. (a) WRF-Chem- and (b) CAM-simulated spatial distribution of AOD over East Asia, the Pacific Ocean, and North America for a dusty day (18 Mar 2011). Model results demonstrate that dust plumes originating in Asia in the beginning of March were transported over a 7-day period to the SPL and AMF sites (not shown). Difference between the WRF-Chem- and CAM-simulated spatial distributions can be attributed to several factors, including specification of major sources and particle size representations (Zhao et al. 2013).

Validation Experiment (STORMVEX) indicates that during March 2011 a major dust event occurred both at the high-elevation, mountain-top SPL, the Atmospheric Radiation Measurement (ARM) Climate Research Facility Mobile Facility located nearby (~2.4 km away), and at the nearest AERONET site located in the vicinity SPL (~150 km away). Output from the high-resolution Weather Research and Forecasting (WRF) Model coupled with chemistry (WRF-Chem; Hu et al. 2016) shows that the dust event is likely associated with transpacific transport of Asian and African plumes, although more work is needed to quantify the contribution. Satellite data, namely MODIS and MISR AOD and CALIOP-derived plume height, provide the observational support of the WRF-Chem simulations. We demonstrate that the coarse mode (volume median diameter ~3 μm) is well defined at the SPL and the nearest AERONET sites despite expected frequent orographic precipitation over mountainous regions in the western United States (Creamean et al. 2013) that may result in significant wet deposition. The importance of the coarse mode contribution to aerosol microphysical and optical properties during the dust event is also demonstrated. For example, the contribution of supermicron particles to the near-surface total scattering coefficient is about 40% and can exceed 70% for the total volume.

Understanding the effects of dust on the regional and global climate requires detailed information on particle size distributions and their changes with distance from the source (Mahowald et al. 2014). Awareness is now growing about the tendency of the dust coarse mode with moderate (~3.5 μm ± 30%) volume median diameter to be rather insensitive to complex removal processes associated with long-range transport of dust from the major sources (Maring et al. 2003; Reid et al. 2008; Ryder et al. 2013). Our study, with a focus on the transpacific transport of the Asian and African dust, complements these previous studies by indicating that the quasi-static nature of the coarse mode appears to be a reasonable approximation for Asian and African dust as well. Since our results rely on 1-month integrated observations at two nearby mountain-top sites, additional efforts with both observational and modeling components are required. However, if the projected robustness of the coarse mode during long-range transport is confirmed, it will become easier to draw conclusions about the dust-related effects of climate change at both the regional and global scales (Richardson et al. 2007; Prenni et al. 2009).

Acknowledgments. This research was supported by the U.S. Department of Energy, Office of Science, Biological

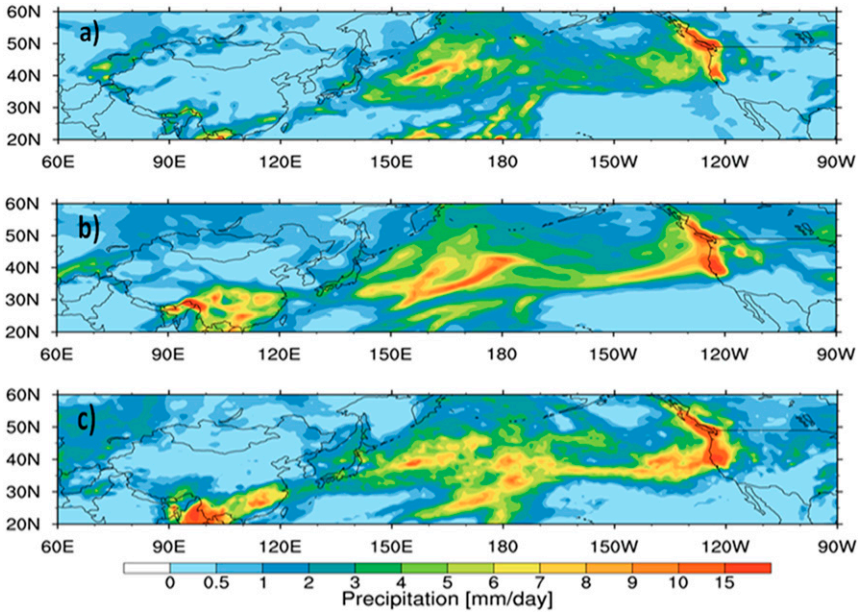

FIG. A2. Spatial distribution of precipitation averaged over the period of interest (11–18 Mar 2011) from (a) the WRF-Chem simulations, (b) CAM5, and (c) the Global Precipitation Climatology Project (GPCP).

and Environmental Research as part of the Atmospheric Radiation Measurement (ARM), Atmospheric System Research (ASR), Earth System Modeling (ESM), and Regional and Global Climate Modeling (RGCM) Programs. The Pacific Northwest National Laboratory is operated by Battelle Memorial Institute under Contract DE-AC06-76RLO 1830. The StormVEx campaign was supported by the ARM and ASR Programs. The Desert Research Institute's SPL is a permitee of the Medicine Bow–Routt National Forests. We would like the following people who made this field campaign possible, including DOE ATSC and ASR staff, SPL local volunteers, the Steamboat Ski and Resort Corporation, the U.S. Forest Service, the Grand Junction National Weather Service office, and graduate students (Betsy Berry, Stewart Evans, Ben Hillman, Will Mace, Clint Schmidt, Carolyn Stwertka, Adam Varble, and Christy Wall), who collected data. We appreciate discussions with Duli Chand, Mikhail Ovchinnikov, and Hailong Wang (PNNL) and two anonymous reviewers for the thoughtful comments.

APPENDIX A

Model Simulations

Dust transport signatures produced in WRF-Chem (Fig. A1a) and CAM5 (Fig. A1b) are broadly similar, but there is a discrepancy in burdens and optical depth suggesting some uncertainty in the quantitative description of transport and removal processes. Sensitivity experiments with and without gravitational sedimentation show that more dust is transported across the Pacific in CAM5 when sedimentation is disabled, producing a simulation more consistent with WRF-Chem (X. Liu 2016, personal communication). One possible explanation for the strong sensitivity to sedimentation in CAM5 is that the dust plume is displaced by sedimentation to lower altitudes, where it is susceptible to stronger wet scavenging. Such sensitivity is not apparent in WRF-Chem, perhaps because of differences in particle size representation (Zhao et al. 2013) and/or wet deposition.

Precipitation along the transport pathway (20°–50°N) is well simulated by the two models (WRF-Chem and CAM5) against observations (Fig. A2). The WRF-Chem simulation produced ~1.8 Tg dust mass outflowed from the western Pacific (20°–50°N, 140°E–120°W) during the period of interest (11–18 March 2011). During the transpacific transport, about 0.5- and 0.2-Tg dust mass are removed by the wet scavenging and dry deposition, respectively. Hence the model simulated more than half of the dust mass outflowed from the western Pacific reaching the western coast of North America. Moreover, over the western United States (20°–50°N, 120°–106°W) during the period of interest (11–18 March 2011), wet and dry deposition removed about 0.03- and 0.19-Tg dust mass, respectively.

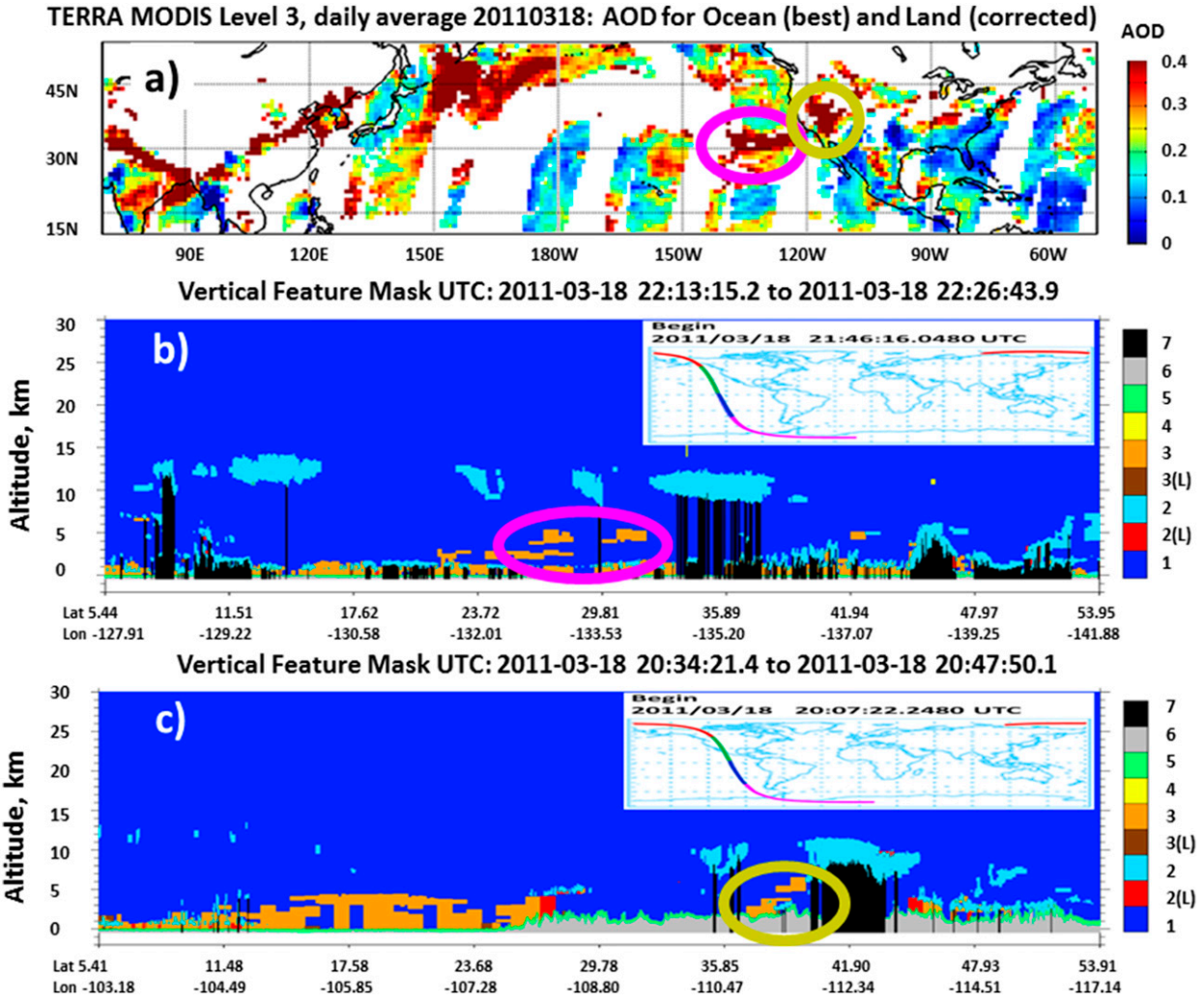

FIG. B1. (a) Spatial distribution of AOD at 0.55-μm wavelength over East Asia, the Pacific Ocean, and North America from MODIS observations (*Terra*, level 3, version 5.1, daily averaged; data from ftp://ladsweb.nascom.nasa.gov/allData/51/MOD08_D3/). Increasing color wavelength (blue to yellow to red) defines increasing values of AOD. Location of aerosol layers over two areas are highlighted by magenta and olive ovals. These areas represent the Pacific Ocean (magenta) and inland (olive) near the coastal line of North America, respectively. The same colors are used to highlight CALIOP-identified (b),(c) elevated aerosol layers. (b),(c) Vertical feature mask (level-1 browse images, version 3.01; nominal daytime) from CALIOP observations. Images in the top-right corners show maps with the corresponding CALIOP overpass with red, green, blue, and magenta sections (from north to south). The selected masks represent green sections of these two overpasses, which are located over (b) the Pacific Ocean and (c) mostly inland near coastal line of North America. Label markers define the following: clear air (1), cloud (2), aerosol (3), stratospheric layer (4), surface (5), subsurface (6), totally attenuated (7), and low or no confidence (L). The CALIOP images from http://www-calipso.larc.nasa.gov/products/lidar/browse_images/show_date.php?s=production&v=V3-01& browse date= 2011-03-18. Both the MODIS AOD and CALIOP mask are obtained for 18 Mar 2011.

APPENDIX B

Satellite-Based Aerosol Properties: Near-Source and Remote Regions

Figure B1 shows aerosol properties obtained from satellite observations in the near-source (East Asia) and remote (the Pacific Ocean and North America) regions. These observations include classification of elevated layers, the so-called vertical feature mask, from the CALIOP lidar on board the *CALIPSO* and aerosol optical depth (AOD) from the MODIS aboard the NASA's *Terra* satellite. Note that AOD is representative of the total aerosol burden in the atmosphere. Based on the multiyear satellite observations, it appears that the transpacific transport of large dust plumes originating from Asia and Africa typically occurred during springtime (Hu et al. 2016). The spring of 2011 was no

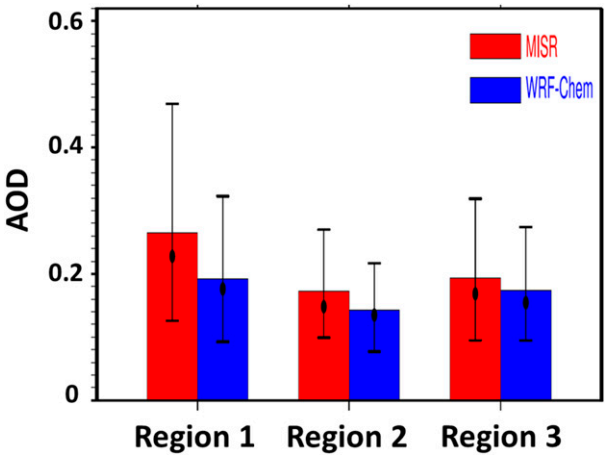

FIG. B2. Mean values (bars) of AOD at 0.55-μm wavelength from satellite retrievals and model simulations over three subregions and the corresponding 10th- and 90th-percentile values (vertical lines). Red and blue colors represent the MISR retrievals and WRF-Chem simulations, respectively.

exception (Fig. B1). In particular, we identify from the MODIS observations in Fig. B1a numerous areas with moderate-to-high (up to 0.4) values of AOD over a large geographical region between Asia and North America for a given day of interest (18 March). The spatial distribution of the MODIS AOD over this region for different days (not shown) indicate that the observed large AODs are associated mostly with dust plumes that originated from Asia and Africa and transported toward North America.

In general, there is a good agreement between the WRF-Chem-simulated (Fig. A1a) and MODIS (Fig. B1a) AODs in terms of their spatial distribution and magnitude. However, there is a moderate underestimation in the WRF-Chem-simulated AOD (Fig. A1a) compared to the MODIS AOD (Fig. B1a). Such underestimation may result from several factors, including the aerosol wet removal applied in the WRF-Chem model and impact of cloud contamination in the MODIS aerosol retrievals (Hu et al. 2016). The elevated aerosol layers are prominent in the CALIOP observations near North America (Figs. B1b,c). The WRF-Chem-simulated total mass of dust (Fig. 5c) has larger values from about 3 to 5 km. This altitude range is consistent with the CALIOP-derived heights (from about 3 to 7 km) of elevated aerosol layers (Fig. B1c) observed near an area surrounding the SPL site.

Following Hu et al. (2016), we also compare AODs from WRF-Chem simulation and satellite retrievals. The MODIS retrievals of AOD in comparison with those from Multiangle Imaging SpectroRadiometer (MISR) observations tend to have larger biases against AERONET-based AOD over land (Hu et al. 2016). Therefore, we select the MISR retrievals for our comparison with the WRF-Chem simulations over the transpacific region (Fig. B2). Similar to Hu et al. (2016), we define three subregions (region 1: 20°–50°N, 120°–140°E; region 2: 20°–50°N, 140°E–140°W; region 3: 20°–50°N, 140°–120°W) for representing the western Pacific, the central Pacific, and the eastern Pacific, respectively. For adequate sampling over the three subregions, we evaluate monthly mean values (March 2011) of AODs. There is a reasonable agreement between the retrieved and simulated AODs (Fig. B2).

APPENDIX C

Ground-Based Aerosol Properties: Near-Source and Remote Regions

Figure C1 shows aerosol properties obtained from AERONET data in near-source (East Asia) and remote (North America) regions. In particular, these data are collected at the SACOL (China, near Taklimakan and Gobi Deserts) and BSRN Boulder Atmospheric Observatory (BAO) (North America) sites. Note that the BSRN BAO site is located about 150 km away from the SPL site. Despite such separation, AODs at the SPL (Fig. 2a) and Boulder (Fig. C1b) sites show similar trends: small (<0.1) values of AOD are followed by a peak on 18 March with the subsequent decrease. There is only one exception (Fig. C1b): a peak (~0.24) on 8 March at the Boulder site indicates a large concentration of small particles given a large AE (~1.26). These similar AOD trends (SPL site vs Boulder site) together with the provided evidence of the major dust episode at the SPL site (section 3) on 18 March suggest that the same dust event is likely detected at these two sites simultaneously.

The simulations reveal that the travel time of dust from the major Asian sources to area surrounding the SPL site is about 1 week (appendix A). Thus, Fig. C1 includes aerosol properties collected at the SACOL site a week before "dusty" day (18 March) at the SPL and Boulder sites. The day of interest (11 March) at the SACOL site is characterized by large (~0.4) and small (~0.4) values of AOD and AE, respectively (Fig. C1a). The observed small value of AE (Fig. C1a) arises from the weak spectral dependence of the corresponding AOD (Fig. C1c), which in turn is caused by large fraction of the supermicron particles in the volume size distribution (Fig. C1d). It should be emphasized that the corresponding values of the VMD is about 5 and 3 μm for the supermicron particles at the SACOL and Boulder sites (Fig. C1d), respectively. The observed VMD value (~5 μm) at SACOL site on 11 March is in a good agreement with the corresponding springtime climatological values (Chen et al. 2014). It is quite interesting that the observed

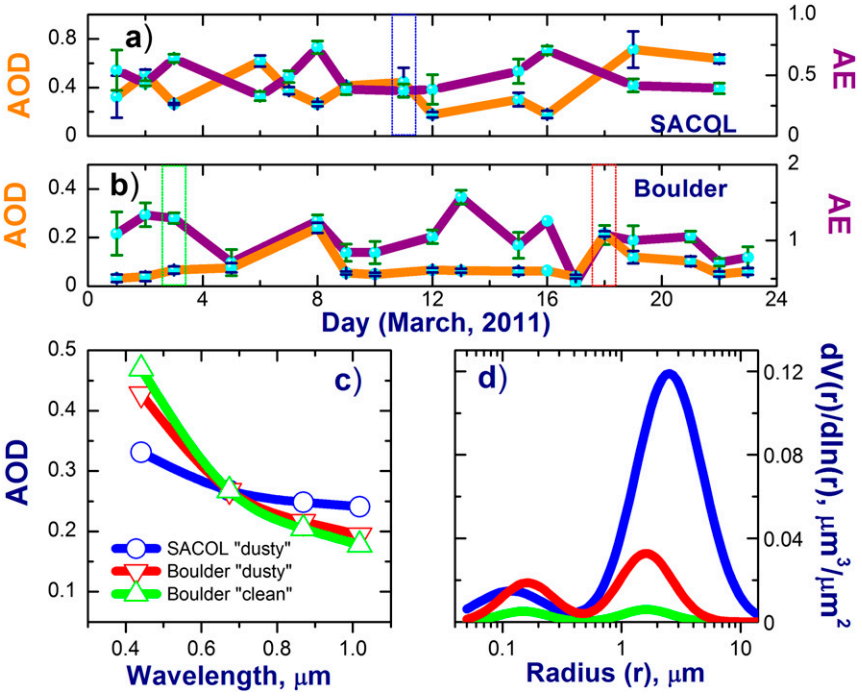

FIG. C1. (a),(b) Column aerosol properties derived from AERONET data (level 2.0; aerosol optical depth V2 product) collected at (a) SACOL site (35.946°N, 104.137°E, 1965 m MSL) and (b) BSRN BAO site (40.045°N, 105.006°W; 1604 m MSL): Time series of daily averaged AOD at 0.5-μm wavelength (orange solid line) and AE (0.44/0.87 μm) (purple solid line). Dusty day with large AOD (11 Mar) at the SACOL site in (a) together with clean (3 Mar) and dusty (18 Mar) days with low and moderate AOD at the Boulder site in (b) are identified by vertical thin lines. The corresponding spectrally resolved (c) AODs and (d) size distributions derived from AERONET data (level 2.0; aerosol inversion V2 product) are included as well: SACOL dusty (blue lines), Boulder dusty (red lines), and Boulder clean (green lines) days. The Boulder AODs for the selected clean and dusty days in (b) are small in comparison with the SACOL dusty AOD in (a). To ease the comparison of the spectral dependence of these AODs, the Boulder AODs are scaled to match the SACOL dusty AOD at 0.674-μm wavelength.

columnar VMD value ($\sim$3 μm) at the Boulder site on 18 March is comparable with the corresponding near-surface value at the SPL site (Fig. 6c).

REFERENCES

Burton, S. P., and Coauthors, 2015: Observations of the spectral dependence of linear particle depolarization ratio of aerosols using NASA Langley airborne High Spectral Resolution Lidar. *Atmos. Chem. Phys.*, **15**, 13 453–13 473, doi:10.5194/acp-15-13453-2015.

Cazorla, A., R. Bahadur, K. J. Suski, J. F. Cahill, D. Chand, B. Schmid, V. Ramanathan, and K. A. Prather, 2013: Relating aerosol absorption due to soot, organic carbon, and dust to emission sources determined from in-situ chemical measurements. *Atmos. Chem. Phys.*, **13**, 9337–9350, doi:10.5194/acp-13-9337-2013.

Chen, S., and Coauthors, 2014: Regional modeling of dust mass balance and radiative forcing over East Asia using WRF-Chem. *Aeolian Res.*, **15**, 15–30, doi:10.1016/j.aeolia.2014.02.001.

Choobari, O. A., P. Zawar-Reza, and A. Sturman, 2014: The global distribution of mineral dust and its impacts on the climate system: A review. *Atmos. Res.*, **138**, 152–165, doi:10.1016/j.atmosres.2013.11.007.

Clarke, A. D., W. G. Collins, P. J. Rasch, V. N. Kapustin, K. Moore, S. Howell, and H. E. Fuelberg, 2001: Dust and pollution transport on global scales: Aerosol measurements and model predictions. *J. Geophys. Res.*, **106**, 32 555–32 569, doi:10.1029/2000JD900842.

Cottle, P., K. Strawbridge, I. McKendry, N. O'Neill, and A. Saha, 2013: A pervasive and persistent Asian dust event over North America during spring 2010: Lidar and sunphotometer observations. *Atmos. Chem. Phys.*, **13**, 4515–4527, doi:10.5194/acp-13-4515-2013.

Creamean, J. M., and Coauthors, 2013: Dust and biological aerosols from the Sahara and Asia influence precipitation in the western U.S. *Science*, **339**, 1572–1578, doi:10.1126/science.1227279.

de Foy, B., S. P. Burton, R. A. Ferrare, C. A. Hostetler, J. W. Hair, C. Wiedinmyer, and L. T. Molina, 2011: Aerosol plume transport and transformation in high spectral resolution lidar measurements and WRF-Flexpart simulations during the MILAGRO Field Campaign. *Atmos. Chem. Phys.*, **11**, 3543–3563, doi:10.5194/acp-11-3543-2011.

Eloranta, E. W., 2005: High spectral resolution lidar. *Lidar: Range-Resolved Optical Remote Sensing of the Atmosphere*, K. Weitkamp, Ed., Springer, 143–163.

Fan, J., and Coauthors, 2014: Aerosol impacts on California winter clouds and precipitation during CalWater 2011: Local pollution versus long-range transported dust. *Atmos. Chem. Phys.*, **14**, 81–101, doi:10.5194/acp-14-81-2014.

Hallar, A. G., R. Petersen, E. Andrews, J. Michalsky, I. B. McCubbin, and J. A. Ogren, 2015: Contributions of dust and biomass burning to aerosols at a Colorado mountain-top site. *Atmos. Chem. Phys.*, **15**, 13 665–13 679, doi:10.5194/acp-15-13665-2015.

Harrison, L., J. Michalsky, and J. Berndt, 1994: Automated multifilter rotating shadow-band radiometer: An instrument for optical depth and radiation measurements. *Appl. Opt.*, **33**, 5118–5125, doi:10.1364/AO.33.005118.

Holben, B. N., and Coauthors, 1998: AERONET—A federated instrument network and data archive for aerosol characterization. *Remote Sens. Environ.*, **66**, 1–16, doi:10.1016/S0034-4257(98)00031-5.

Hu, Z., C. Zhao, J. Huang, L. R. Leung, Y. Qian, H. Yu, L. Huang, and O. V. Kalashnikova, 2016: Trans-Pacific transport and evolution of aerosols: Evaluation of quasi-global WRF-Chem simulation with multiple observations. *Geosci. Model Dev.*, **9**, 1725–1746, doi:10.5194/gmd-9-1725-2016.

Kinne, S., and Coauthors, 2006: An AeroCom initial assessment—Optical properties in aerosol component modules of global models. *Atmos. Chem. Phys.*, **6**, 1815–1834, doi:10.5194/acp-6-1815-2006.

Lack, D. A., and C. D. Cappa, 2010: Impact of brown and clear carbon on light absorption enhancement, single scatter albedo and absorption wavelength dependence of black carbon. *Atmos. Chem. Phys.*, **10**, 4207–4220, doi:10.5194/acp-10-4207-2010.

Levy, R. C., S. Mattoo, L. A. Munchak, L. A. Remer, A. M. Sayer, F. Patadia, and N. C. Hsu, 2013: The Collection 6 MODIS aerosol products over land and ocean. *Atmos. Meas. Tech.*, **6**, 2989–3034, doi:10.5194/amt-6-2989-2013.

Liu, X., and Coauthors, 2012: Toward a minimal representation of aerosols in climate models: Description and evaluation in the Community Atmosphere Model CAM5. *Geosci. Model Dev.*, **5**, 709–739, doi:10.5194/gmd-5-709-2012.

Ma, P.-L., and Coauthors, 2015: How does increasing horizontal resolution in a global climate model improve the simulation of aerosol-cloud interactions? *Geophys. Res. Lett.*, **42**, 5058–5065, doi:10.1002/2015GL064183.

Mahowald, N., S. Albani, J. F. Kok, S. Engelstaeder, R. Scanza, D. S. Ward, and M. G. Flanner, 2014: The size distribution of desert dust aerosols and its impact on the Earth system. *Aeolian Res.*, **15**, 53–71, doi:10.1016/j.aeolia.2013.09.002.

Malm, W. C., J. F. Sisler, D. Huffman, R. A. Eldred, and T. A. Cahill, 1994: Spatial and seasonal trends in particle concentration and optical extinction in the United States. *J. Geophys. Res.*, **99**, 1347–1370, doi:10.1029/93JD02916.

Marchand, R., G. G. Mace, A. G. Hallar, I. B. McCubbin, S. Y. Matrosov, and M. D. Shupe, 2013: Enhanced radar backscattering due to oriented ice particles at 95 GHz during StormVEx. *J. Atmos. Oceanic Technol.*, **30**, 2336–2351, doi:10.1175/JTECH-D-13-00005.1.

Maring, H., D. L. Savoie, M. A. Izaguirre, L. Custals, and J. S. Reid, 2003: Mineral dust aerosol size distribution change during atmospheric transport. *J. Geophys. Res.*, **108**, 8592, doi:10.1029/2002JD002536.

Michalsky, J., F. Denn, C. Flynn, G. Hodges, P. Kiedron, A. Koontz, J. Schlemmer, and S. E. Schwartz, 2010: Climatology of aerosol optical depth in north-central Oklahoma: 1992–2008. *J. Geophys. Res.*, **115**, D07203, doi:10.1029/2009JD012197.

Nowottnick, E., P. Colarco, A. da Silva, D. Hlavka, and M. McGill, 2011: The fate of Saharan dust across the Atlantic and implications for a Central American dust barrier. *Atmos. Chem. Phys.*, **11**, 8415–8431, doi:10.5194/acp-11-8415-2011.

Obrist, D., A. G. Hallar, I. McCubbin, B. B. Stephens, and T. Rahn, 2008: Atmospheric mercury concentrations at Storm Peak Laboratory in the Rocky Mountains: Evidence for long-range transport from Asia, boundary layer contributions, and plant mercury uptake. *Atmos. Environ.*, **42**, 7579–7589, doi:10.1016/j.atmosenv.2008.06.051.

Pan, X., and Coauthors, 2015: Observation of the simultaneous transport of Asian mineral dust aerosols with anthropogenic pollutants using a POPC during a long-lasting dust event in late spring 2014. *Geophys. Res. Lett.*, **42**, 1593–1598, doi:10.1002/2014GL062491.

Prenni, A. J., and Coauthors, 2009: Relative roles of biogenic emissions and Saharan dust as ice nuclei in the Amazon basin. *Nat. Geosci.*, **2**, 402–405, doi:10.1038/ngeo517.

Rasch, P., and Coauthors, 2000: A comparison of scavenging and deposition processes in global models: Results from the WCRP Cambridge Workshop of 1995. *Tellus*, **52B**, 1025–1056, doi:10.3402/tellusb.v52i4.17091.

Reid, J. S., E. A. Reid, A. Walker, S. Piketh, S. Cliff, A. Al Mandoos, S.-C. Tsay, and T. F. Eck, 2008: Dynamics of southwest Asian dust particle size characteristics with implications for global dust research. *J. Geophys. Res.*, **113**, D14212, doi:10.1029/2007JD009752.

Richardson, M. S., and Coauthors, 2007: Measurements of heterogeneous ice nuclei in the western United States in springtime and their relation to aerosol characteristics. *J. Geophys. Res.*, **112**, D02209, doi:10.1029/2006JD007500.

Ryder, C. L., E. J. Highwood, T. M. Lai, H. Sodemann, and J. H. Marsham, 2013: Impact of atmospheric transport on the evolution of microphysical and optical properties of Saharan dust. *Geophys. Res. Lett.*, **40**, 2433–2438, doi:10.1002/grl.50482.

Slingo, A., and Coauthors, 2006: Observations of the impact of a major Saharan dust storm on the atmospheric radiation balance. *Geophys. Res. Lett.*, **33**, L24817, doi:10.1029/2006GL027869.

Wang, X., L. Zhang, and M. D. Moran, 2014: Bulk or modal parameterizations for below-cloud scavenging of fine, coarse, and giant particles by both rain and snow. *J. Adv. Model. Earth Syst.*, **6**, 1301–1310, doi:10.1002/2014MS000392.

Wells, K. C., M. Witek, P. Flatau, S. M. Kreidenweis, and D. L. Westphal, 2007: An analysis of seasonal surface dust aerosol concentrations in the western US (2001–2004): Observations and model predictions. *Atmos. Environ.*, **41**, 6585–6597, doi:10.1016/j.atmosenv.2007.04.034.

Winker, D., M. Vaughan, A. Omar, Y. Hu, K. Powell, Z. Liu, W. Hunt, and S. Young, 2009: Overview of the CALIPSO mission and CALIOP data processing algorithms. *J. Atmos. Oceanic Technol.*, **26**, 2310–2323, doi:10.1175/2009JTECHA1281.1.

Zelenyuk, A., D. Imre, J. Wilson, Z. Zhang, J. Wang, and K. Mueller, 2015: Airborne Single Particle Mass Spectrometers (SPLAT II & miniSPLAT) and new software for data visualization and analysis in a geo-spatial context. *J. Amer. Soc. Mass Spectrom.*, **26**, 257–270, doi:10.1007/s13361-014-1043-4.

Zhao, C., S. Chen, L. R. Leung, Y. Qian, J. F. Kok, R. A. Zaveri, and J. Huang, 2013: Uncertainty in modeling dust mass balance and radiative forcing from size parameterization. *Atmos. Chem. Phys.*, **13**, 10 733–10 753, doi:10.5194/acp-13-10733-2013.